Journal of Applied Polymer Science

Cassava starch-based nanocomposites reinforced with cellulose nanofibers extracted from sisal

Jamille Santos Santana,[1] Jamile Marques do Rosário,[2] Cícero Cardoso Pola,[3] Caio Gomide Otoni,[4] Nilda de Fátima Ferreira Soares,[3] Geany Peruch Camilloto,[2] Renato Souza Cruz[1,2]

[1]Department of Chemical Analyses, Faculty of Pharmacy, Graduate Program in Food Science, Federal University of Bahia (UFBA), Rua Barão de Jeremoabo, s/n, Salvador, BA 40170-110, Brazil

[2]Department of Technology, Faculty of Food Engineering, Feira de Santana State University (UEFS), Av. Transnordestina, s/n, Feira de Santana, BA 44036-900, Brazil

[3]Department of Food Technology, Laboratory of Food Packaging, Federal University of Viçosa (UFV), Av. PH Rolfs, s/n, Viçosa, MG 36570-900, Brazil

[4]Department of Materials Engineering, Federal University of São Carlos (UFSCar), PPG-CEM, Rodovia Washington Luís, Km 235, São Carlos, SP 13566-905, Brazil

Correspondence to: R. S. Cruz (E-mail: cruz.rs@uefs.br)

ABSTRACT: Cellulose nanofibers were extracted from sisal and incorporated at different concentrations (0–5%) into cassava starch to produce nanocomposites. Films' morphology, thickness, transparency, swelling degree in water, water vapor permeability (WVP) as well as thermal and mechanical properties were studied. Cellulose nanofiber addition affected neither thickness (56.637 ± 2.939 μm) nor transparency (2.97 ± 1.07 mm^{-1}). WVP was reduced until a cellulose nanofiber content of 3.44%. Tensile force was increased up to a nanocellulose concentration of 3.25%. Elongation was decreased linearly upon cellulose nanofiber addition. Among all films, the greatest Young's modulus was 2.2 GPa. Cellulose nanofibers were found to reduce the onset temperature of thermal degradation, although melting temperature and enthalpy were higher for the nanocomposites. Because cellulose nanofibers were able to improve key properties of the films, the results obtained here can pave the route for the development and large-scale production of novel biodegradable packaging materials. © 2016 Wiley Periodicals, Inc. J. Appl. Polym. Sci. **2017**, *134*, 44637.

KEYWORDS: biopolymers and renewable polymers; cellulose and other wood products; composites; packaging; polysaccharides

Received 17 July 2016; accepted 7 November 2016

DOI: 10.1002/app.44637

INTRODUCTION

Nonrenewable synthetic materials play an important role in modern society, but these are being increasingly associated with remarkable environmental problems as a result of the accumulation of non-biodegradable plastics.[1] Obtaining biodegradable materials exhibiting thermoplastic properties from renewable sources (e.g., starch and cellulose) denotes a means of reducing the environmental impact caused by the intense use of petroleum-derived materials.[2–6] In this context, starch has been pointed out as a feasible alternative for plastics derived from fossil sources,[7–9] mainly because it is renewable, widely available in nature, and inexpensive.

Starch comprises two polysaccharides derived from α-D-glucose: amylose and amylopectin. In its native form, starch features a granular structure, which may be transformed into a continuous phase, named thermoplastic starch (TPS).[10] This can be achieved through the input of thermal and/or mechanical energy together with the addition of a plasticizer, i.e., a substance capable of modifying starch molecular network in a way that increases its free volume.[11] Plasticized starch still presents some limitations, including high affinity to water (and, thus, water absorption) as well as weak mechanical properties, the latter being strongly affected by relative humidity (RH).[12] Therefore, the addition of cellulose nanofibers stands out as a promising strategy to overcome this hurdle.[13,14]

Cellulose nanofibers are crystalline domains featuring unique physical characteristics: stiffness, thickness, and length.[15] These highly oriented structures lead not only to more resistant materials, but also to materials having distinct optical, magnetic, electrical, and conductivity properties if compared to the macroscopic material.[16]

Nanofibers may be obtained from numerous lignocellulosic sources, including coconut husk,[17] cassava bagasse,[18] eucalyptus

wood,[19] and cotton linter.[20] One of the most common methods for nanofiber extraction relies upon cellulose hydrolysis by a strong acid (e.g., sulfuric acid or hydrochloric acid).[21]

Numerous studies have investigated the influence of cellulose nanofibers on the physical properties of nanocomposites based on starch,[22] agar,[23] and poly(vinyl alcohol) (PVA),[24] to mention a few. In these studies, the addition of nanocellulose has been demonstrated to be a promising approach for improving the performance of nanocomposite films, especially concerning their mechanical properties. Alves *et al.*[22] reported that nanocellulose successfully improved the mechanical properties of corn starch-based films. Similarly, Lee *et al.*[24] observed that the addition of nanocellulose led to increased tensile strength in PVA-based composites. Most studies, however, are concerned only the reinforcement effect of nanocellulose on the mechanical properties of polymer-based composites. Here, glycerol-plasticized cassava starch-based nanocomposites incorporated with cellulose nanofibers extracted from sisal were produced. Although the resulting materials showed improved mechanical properties upon the addition of nanocellulose, similarly to previous reports, we also investigated the effects of this nano-sized filler on the morphology as well as the swelling, thermal, and water barrier properties of the nanocomposites. Indeed, enhanced water barrier and thermal properties were achieved as well.

EXPERIMENTAL

Materials

Cassava starch (amylose content: 32.5 ± 0.3%; solubility index: 0.314 ± 0.076%; water absorption: 1.766 ± 0.076%; density: 1.544 ± 0.023 g cm^{-3}) and sisal fibers were kindly provided by Bahiamido Serviços Agroindustriais S.A. (Santo Antônio de Jesus, BA, Brazil) and APAEB—*Associação para o Desenvolvimento Sustentável e Solidariedade* (Valente, BA, Brazil), respectively. Sodium hydroxide, acetic acid, sulfuric acid, sodium chlorite, and glycerol were purchased from Sigma Aldrich (São Paulo, SP, Brazil).

Cellulose Extraction

Cellulose was extracted in accordance with a methodology adapted from da Silva *et al.*[19] Sisal fibers were washed with distilled water and dried at 40 °C for 24 hr in order to increase the efficiency of future alkali attack. Then, fibers were macerated with a 2% (w v^{-1}) NaOH solution undergoing mechanical stirring at 80 °C for 4 hr, procedure which was repeated four times—fibers were filtered and washed with distilled water between each maceration cycle. Then, each 10 g of cellulose fibers was bleached with a solution containing 100 mL of aqueous $NaClO_2$ 1.7% (w v^{-1}) and 100 mL of acetate buffer (27 g of NaOH and 75 mL of glacial acetic acid, diluted to 1 L with distilled water). The mixture was maintained at 80 °C for 6 hr and the process was repeated twice—likewise, fibers were filtered and washed between each repetition. The extracted cellulose was kiln dried at 40 °C for 48 hr and then crushed.

Cellulose Nanofiber Extraction

Cellulose nanofibers were extracted via acid hydrolysis using a 64% (v v^{-1}) sulfuric acid solution. The extraction protocol has been described in details by Sammir *et al.*[16] Briefly, it relied upon the acid-insolubility of crystalline domains at the conditions which they experienced. This is due to the inaccessibility of acid within the highly organized, crystalline domains of cellulose molecules. Furthermore, the disruption of native cellulose molecules in their amorphous regions favors the accessibility of acid and, consequently, the hydrolysis of amorphous cellulose chains. Here, 15 mL g^{-1} of sulfuric acid was added to cellulose, concentration which assisted fiber dispersion within the acid. This mixture was stirred at 45 °C for 10 min. Right after hydrolysis, the suspension was diluted (1:1) in cold water and washed by centrifugation (2709*g*) at 10 °C for 20 min. These steps were repeated until the supernatant became turbid. Then, it was subjected to dialysis for 7 days until a pH value between 6 and 7 was reached. The nanofiber solution was sonicated at 140 Hz for 20 min and then cold-stored at 10 °C.[19]

Transmission Electron Microscopy (TEM)

TEM images of cellulose nanofibers were obtained in a JEOL EM 12130 microscope, according with da Silva *et al.*[19]: one drop of an aqueous nanofiber solution (0.3%) was deposited onto a nickel grid (200 mesh). Once dried, the grid was stained with a 2% uranyl acetate solution and then dried at room condition. Samples were imaged at 80 kV.

Zeta Potential and Particle Size

Dynamic and electrophoretic light scatterings were used to determine nanofiber average dimensions and zeta potentials, respectively, in a Zetasizer Nano Series (Malvern Instruments Ltd., UK). The analyzed samples comprised 0.3% aqueous nanofiber suspensions.

Nanocomposite Preparation

The nanocomposites were prepared through casting.[7] To do so, 6% (w v^{-1}) of cassava starch, 8% (w w_{starch}^{-1}) of glycerol, and 0 (F0), 1 (F1), 3 (F3), or 5% (w w_{starch}^{-1}) (F5) of cellulose nanofibers were diluted in water to form film-forming solutions (FFSs). The FFSs were heated up to starch gelatinization temperature (70 °C) undergoing gentle stirring and then spread onto glass plates. The FFSs were kiln dried at 32 °C for 24 hr. Dried films were stored at 10 °C until used for testing.

Scanning Electron Microscopy (SEM)

The morphology of the nanocomposites—previously coated with a thin gold layer—was analyzed in a digital scanning electron microscope (Leo 1430VP, Germany), in accordance with a methodology adapted from Liu *et al.*[9] SEM images of films' surfaces and cryofractured cross sections were obtained using 10 and 15 kV, respectively.

Thickness

The thicknesses of the nanocomposites were measured to the nearest 0.001 mm with a digital micrometer (Mitutoyo America Corporation, USA). Ten random measurements throughout the films were averaged.[7]

Transparency

The transmittances of the nanocomposites were measured in a UV-visible spectrophotometer at wavelengths ranging from 200 to 800 nm, as previously described in the literature.[25,26] Transparency was calculated by eq. (1)[27]:

$$\text{Transparency} = -\frac{\text{Log } T_{600}}{\text{Thickness}} \quad (1)$$

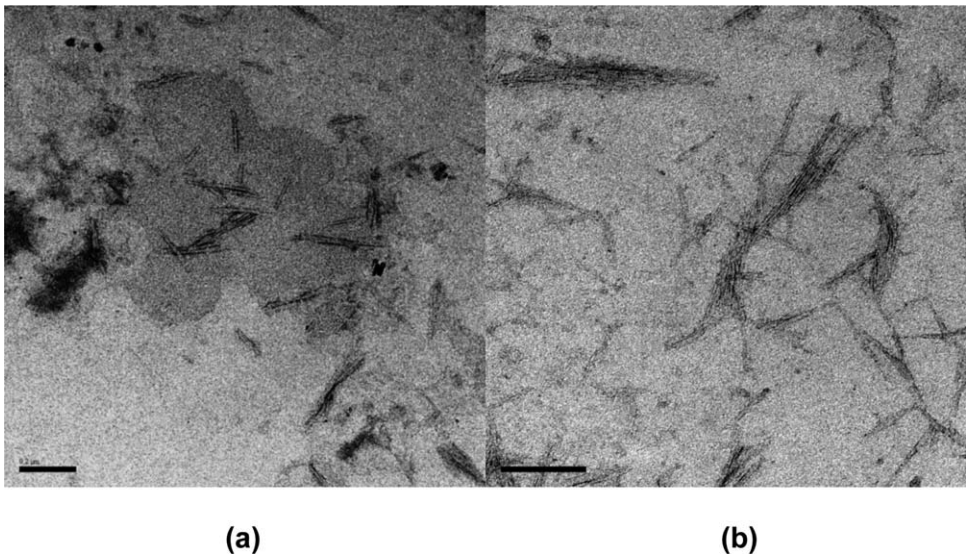

Figure 1. Transmission electron microscopy images of an aqueous suspension of cellulose nanofibers extracted from sisal (bar = 200 nm).

where T_{600} is the transmittance at 600 nm.

Higher transparency values indicate less transparent—i.e., more opaque—films.[28]

Swelling Degree in Water

Swelling degree was determined according with a methodology adapted from Jipa, Stoica-Guzun, and Stroescu.[29] The nanocomposites were shaped into 2 × 2 cm^2 specimens, in triplicates, and dried until constant weight. Film samples were immersed in distilled water at room temperature for 2 hr and then the excess water on sample surfaces was removed. Swelling degree was calculated by eq. (2).

$$\text{Swelling degree} = \frac{m_s - m_i}{m_i} \times 100 \quad (2)$$

where m_i is the initial mass and m_s is the mass of the swollen sample.

Water Barrier Properties

Water vapor transmission rate (WVTR) and permeability (WVP) were determined, in duplicates, through the gravimetric method recommended by ASTM E96/E96M-12.[30] Film samples were fixed to capsules containing $CaCl_2$—as a hygroscopic substance—and sealed with paraffin to ensure that moisture diffusion took place exclusively through the film. The system was placed in a desiccator at 25 °C and 75% RH, the latter being ensured by a saturated NaCl solution. Weight increase was monitored daily (two measurements a day separated by a suitable period of time) for 14 days and was attributed to water diffusion. WVTR through the samples was calculated by eq. (3):

$$\text{WVTR} = \frac{g}{t\,A} \quad (3)$$

where A is the area available for permeation, g is the gained weight, and t is time (h).

The term g t^{-1} was obtained through linear regression, whereas WVP was calculated by eq. (4).

$$\text{WVP} = \frac{\text{WVT}R.\ t}{\text{ps.}(\text{RH}_1 - \text{RH}_1)} \quad (4)$$

where e is the sample average thickness (mm), ps is the steam saturation pressure at the test temperature (kPa), and RH_1 and RH_2 are the relative humidity values within the chamber and the capsule (%), respectively.

Mechanical Properties

The mechanical properties were evaluated in a TA.XT Plus texturometer, in accordance with the standard method ASTM 638–09.[31] The nanocomposites were shaped into 12.5 × 2.5 cm^2 strips and mounted in grips that were initially separated by 50 mm and then stretched the samples at 5.0 mm min^{-1}. The mechanical attributes tensile force (N), elongation at break (%), and Young's modulus (MPa) were determined.

The same equipment was used to perform the puncture assay in order to determine the puncture force (N). In this test, a 6 mm diameter cylindrical probe penetrated the samples up to 10 mm at pretest and test speeds of 2 and 1 mm s^{-1}, respectively, until film surface was fractured. The puncture force was determined according with ASTM F1306–90(2008)e1.[32]

Thermogravimetry (TG)

The thermal events of both nanocomposite films and nanofibers were investigated in a thermal analyzer Shimadzu DTG–60H, at a heating rate of 10 °C min^{-1} and under an inert atmosphere comprising N_2 flowing at 30 mL min^{-1}. Approximately 5 mg of film was heated from 25 to 600 °C, and the weight was monitored as a function of temperature.[33]

Differential Scanning Calorimetry (DSC)

A methodology adapted from Detduangchan *et al.*[8] was used for DSC runs in a Shimadzu DSC–60. Around 5 mg of film samples previously conditioned to 60% RH and 25 °C) was air tightly sealed in aluminum crucibles to prevent water evaporation during the measurements. An empty aluminum crucible served as reference. The analysis was carried out in triplicates

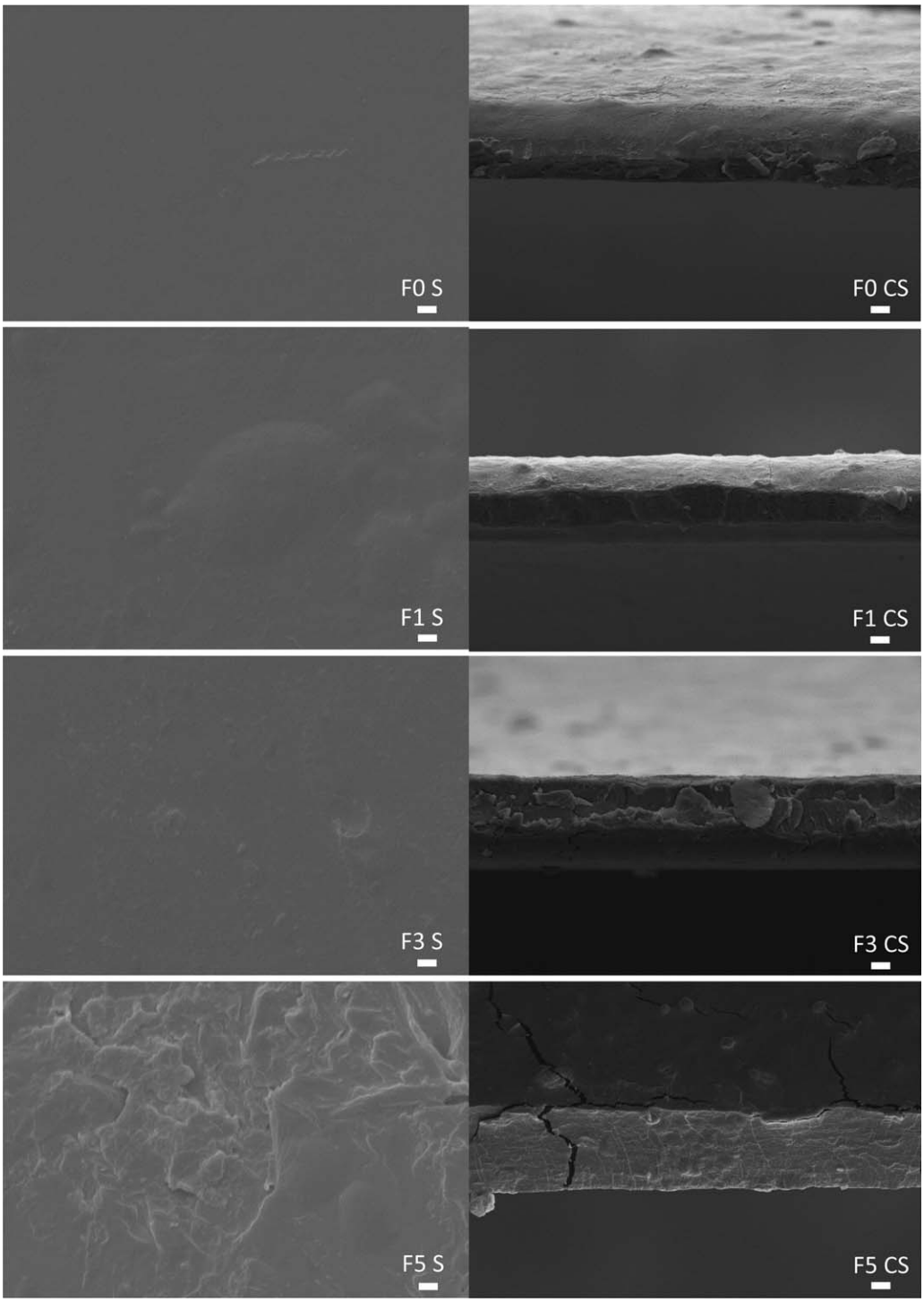

Figure 2. Scanning electron microscopy images of the surfaces (S; bar = 2 μm) and cross sections (CS; bar = 10 μm) of cassava starch-based nanocomposites added by glycerol and 0 (F0), 1 (F1), 3 (F3), or 5% (F5) of cellulose nanofibers extracted from sisal.

and the temperature ranged from −50 to 250 °C at a rate of 10 °C min^{-1} within a N_2 flow of 10 mL min^{-1}.

Statistical Analyses

This study was performed in a completely randomized design, with three repetitions. Analysis of variance (ANOVA) at 95% of confidence level was applied to film's thickness, transparency, swelling degree, mechanical attributes, and WVP. The SAS software, version 9.1, was used. Results that presented significant variances were fitted with mathematical models through linear ($Y = Ax + B$) or polynomial ($Y = Ax^2 + Bx + C$) regression, as suitable.

RESULTS AND DISCUSSION

Transmission Electron Microscopy (TEM)

Figure 1 shows TEM images of an aqueous suspension of cellulose nanofibers extracted from sisal via acidic hydrolysis. The

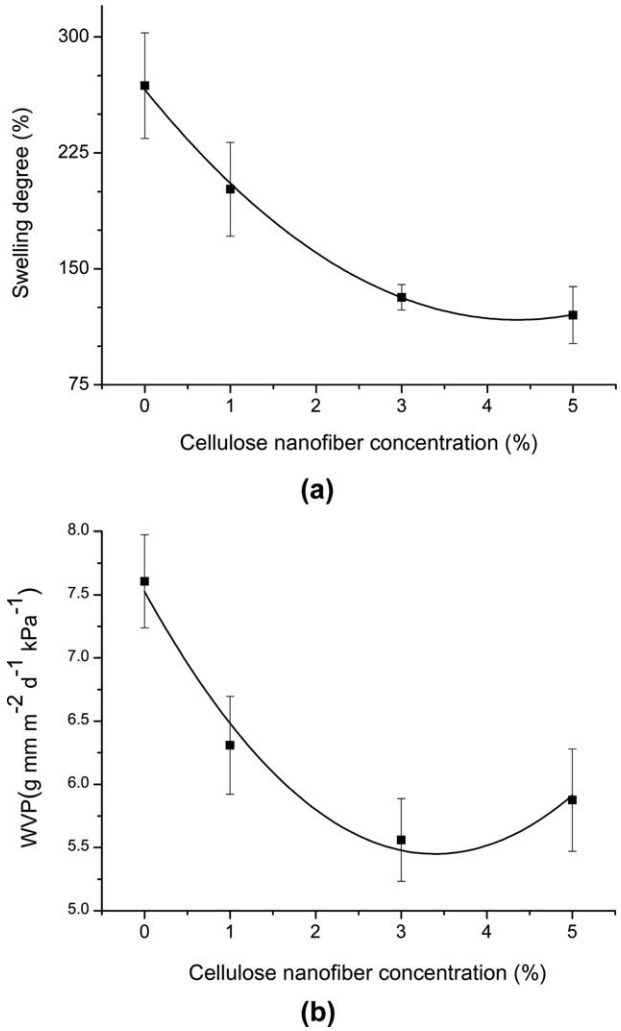

Figure 3. Swelling degree (a) and water vapor permeability (WVP) (b) of cassava-starch based nanocomposites incorporated with glycerol and varying concentrations of cellulose nanofibers extracted from sisal.

extracted procedure led to nanofibers having average length (L) of 302.3 ± 29.2 nm, diameter (D) of 12.7 ± 1.6 nm, and aspect ratio ($L\ D^{-1}$) of 23.9 ± 1.9 nm. Nanofiber clusters can be observed in Figure 1(b). According to Elazzouzi-Hafraoui *et al.*,[34] these clusters are common in cellulose nanofiber aqueous solutions because of their remarkably high surface areas and occurrence of strong hydrogen bonding. This is particularly important when fibers are dried due to a widely known aggregation phenomenon called hornification.

Zeta Potential and Particle Size

Two particle populations featuring different size ranges were observed: one of them comprised 42.9% of the particles and ranged in size from 42.82 to 190.1 nm (average size: 98.99 ± 25.31 nm) whereas 57.1% of the particles remained in the other population, which consisted of particles from 220.2 to 955.4 nm (average size: 455.50 ± 119.30 nm).

Zeta potential measurements were used to estimate the repulsive electrostatic forces among particles and provided an idea of the stability of the cellulose nanofiber suspension. An average zeta potential of −23.6 ± 2.1 mV was found here. According to Zhou *et al.*,[35] the threshold for flocculation or sedimentation of cellulose particles in a suspension is ±15.0 mV, being values higher than ±30.0 mV attributed to a remarkably stable suspension. Thus, the obtained cellulose nanofiber suspension was not highly stable, which may be a result of the shorter hydrolysis time used here when compared to other studies. Still, the net surface charge indicated by zeta potential was large enough to lessen both flocculation and sedimentation.

Scanning Electron Microscopy (SEM)

Figure 2 demonstrates the homogeneous surface of the nanocomposite made up of formulation F1. This was also true for its cross section and indicates proper dispersion and compatibility among the components. Formulation F0 also led to a film exhibiting a cohesive aspect, especially when compared with those from formulations F3 and F5. Formulation F3, particularly, led to a nanocomposite featuring a heterogeneous cross section, which is believed to be a result of the presence of insolubilized polymer portions. According to Espitia *et al.*,[36] this observation denotes the weak interaction of the polymer matrix, which was not able to maintain the integrity of the microscopic surface. Some discontinuities were observed throughout the nanocomposite F5, suggesting a partial miscibility between the formulation components under the processing conditions used. It was also possible to observe the formation of clusters that can be attributable to the poor dispersion of the high contents of cellulose nanofibers within the polymer matrix.

Swelling Degree in Water and Transparency

Cellulose nanofiber concentration affected ($p < 0.05$) the swelling degree in water of the cassava starch-based nanocomposites. The second-order polynomial model $y = 8.27x^2 - 70.59x + 266.86$ ($R^2 = 0.99$) was effective in explaining the behavior of the nanocomposite films upon nanofiber addition. According to this model [Figure 3(a)], the minimum swelling degree (116.23%) would be obtained for a cellulose nanofiber concentration of 4.27%.

Khan *et al.*[37] stated that water absorption by polymer-based composites depends on the nature of both the matrix and the filler. The reduction of the swelling degree in water observed here may be attributed to the high crystallinity of the cellulose nanofibers—making them less hydrophilic than starch—as well as to the strong interactions among the cassava starch matrix and the filler.

ANOVA indicated that cellulose nanofiber concentration did not affect ($p > 0.05$) the transparency of cassava starch-based nanocomposite films. The average values were as follows: 2.30 ± 0.57 (F0), 3.26 ± 1.74 (F1), 2.49 ± 0.68 (F3), and 3.82 ± 0.47 mm^{-1} (F5). This suggests that the addition of cellulose nanofibers would not impair the practical applicability of cassava starch-based films in see-through (transparent) packaging.

Water Vapor Permeability (WVP)

WVP of glycerol-plasticized cassava starch-based films was significantly affected ($p < 0.05$) by the addition of cellulose nanofibers [Figure 3(b)]. The mathematical model fitted by polynomial regression is: $y = 0.18x^2 - 1.24x + 7.52$ ($R^2 = 0.98$). This model

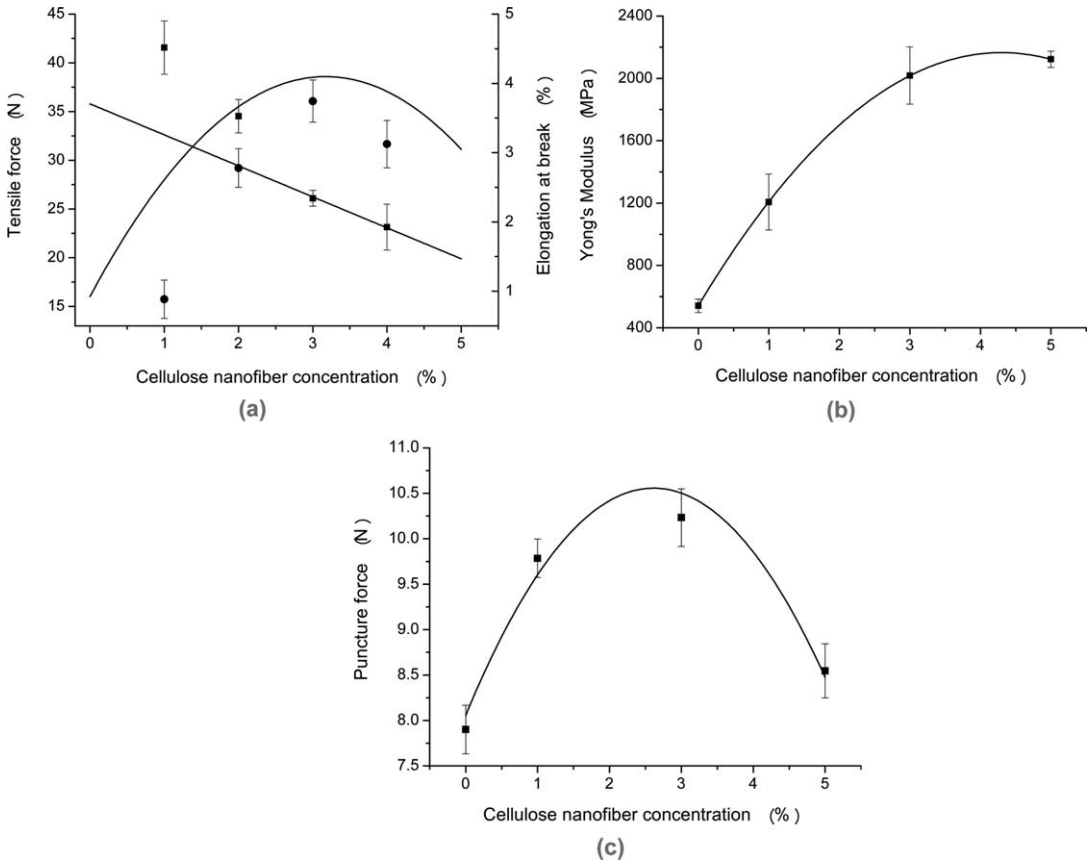

Figure 4. Tensile force (•) and elongation at break (■) (a), Young's modulus (b), and puncture force (c) of cassava-starch based nanocomposites incorporated with glycerol and varying concentrations of cellulose nanofibers extracted from sisal.

shows that the lowest WVP (5.38 g mm m^{-2} d^{-1} kPa^{-1}) would occur for a cellulose nanofiber concentration of 3.44%.

The decreased WVP observed in nanofiber-added structures can be explained by the crystalline domains with a high orientation degree that are formed when these nanoparticles are evenly spread throughout the polymer matrix. These domains act as a labyrinth and prevent the diffusion of water vapor through the matrix by increasing the tortuosity as well as the length of the diffusion pathway.[38,39]

Mechanical Properties

Tensile Force. The incorporation of sisal-extracted cellulose nanofibers significantly influenced ($p < 0.05$) the tensile force of cassava starch-based nanocomposites [Figure 4(a)]. The model that best described this relationship was: $y = -1.96x^2 + 12.75x + 16.67$ ($R^2 = 0.98$). The maximum tensile force (37.40 N) would be observed for a cellulose nanofiber concentration of 3.25%. Higher concentrations tended to decrease the tensile force [Figure 4(a)].

This observation is in accordance with the nonideal zeta potential values found for the nanofibers, implying a tendency to agglomerate. Indeed, agglomeration was observed in SEM images. Agglomerated nanofibers might have led to an uneven tension distribution throughout the nanocomposites and to points where tensile tension was concentrated to a higher extent, which in turn is known to impair the tensile resistance of the composites. This was observed here for cellulose nanofiber concentrations higher than 3.25%.

Elongation at Break. The elongation of the nanocomposites significantly decreased ($p < 0.05$) as cellulose nanofiber content was increased. The mathematical model [Figure 4(a)] obtained for this attribute was: $y = -0.51x + 4.23$ ($R^2 = 0.93$). The addition of nanoparticles caused a linear decrease in nanocomposite elongation. The angular coefficient suggests that each 1% increase in cellulose nanofiber concentration was responsible for a reduction of 0.51% in elongation.

Cellulose nanofibers decreased the elongation of the nanocomposites because they strongly interact with the matrix. According to Chang *et al.*,[33] fillers that have strong interactions with starch macromolecules can improve the tensile strength of the resulting film, but consequently decrease the flexibility of the polymer chains as well as the extensibility of the films.

Young's Modulus. The addition of cellulose nanofibers also influenced significantly ($p < 0.05$) the Young's modulus of the nanocomposites, according to the following mathematical model obtained by polynomial regression [Figure 4(b)]: $y = -87.91x^2 + 755.94x + 540.50$ ($R^2 = 1$). Considering this equation, the maximum Young's modulus (2165.59 MPa) would be found for a cellulose nanofiber concentration of 4.3%.

Kalia *et al.*[40] attributed the increase in the Young's modulus to the stiffness and strength which are typical and inherent to cellulose nanofibers. According to Anglès and Dufresne,[41] some amylopectin chains of starch can crystallize on the surface of

Table I. Temperatures at Which the Thermal Degradation of Cassava-Starch Based Nanocomposites Incorporated with Glycerol and 0 (F0), 1 (F1), 3 (F3), or 5% (F5) of Cellulose Nanofibers Began (T_{onset}), Finished (T_{offset}) and Presented Maximum Rate (T_{peak})

Film	T_{onset} (°C)	T_{peak} (°C)	T_{offset} (°C)	Mass loss (%)
F0	285.09	316.72	344.35	81
F1	273.16	314.28	352.81	80
F3	269.25	295.96	344.42	77
F5	257.46	307.76	340.96	75

Table II. Temperatures at Which Cassava-Starch Based Nanocomposites Incorporated with Glycerol and 0 (F0), 1 (F1), 3 (F3), or 5% (F5) of Cellulose Nanofibers Started to Melt (T_{onset}) and Presented the Highest Melting Rate ($T_{melting}$), as well as the total Heat Absorbed during Melting ($\Delta H_{melting}$)

Film	T_{onset} (°C)	$T_{melting}$ (°C)	$\Delta H_{melting}$ (J/g)
F0	29.63	80.01	252.83
F1	32.11	98.27	314.58
F3	28.74	89.61	343.42
F5	27.97	85.91	298.15

cellulose crystals, leading to increased stiffness as a result of the increased crystallinity.

Puncture Force. The puncture force was also affected ($p < 0.05$) by the addition of cellulose nanofibers. The mathematical model obtained by polynomial regression was: $y = -0.35x^2 + 1.83x + 8.04$ ($R^2 = 0.96$). In accordance with this equation, the maximum puncture force (10.43 N) would occur for a cellulose nanofiber concentration of 2.61% [Figure 4(c)]. For higher concentrations, decreased puncture forces were observed. These results are consistent with those obtained in the tensile assay. Similarly, a decrease in the maximum tensile force was observed from a certain concentration of cellulose nanofibers on, probably because of the presence of nanofiber clusters.

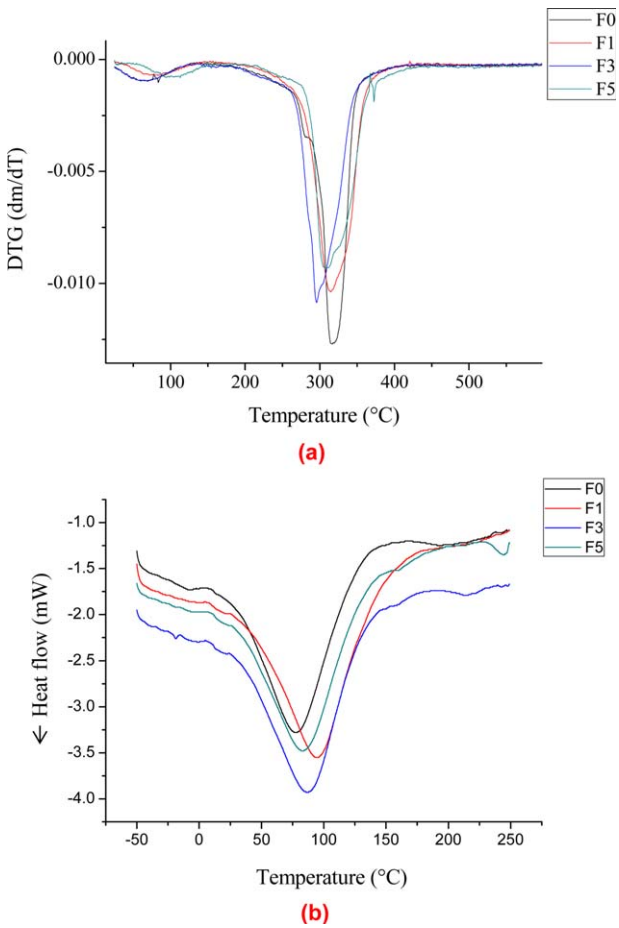

Figure 5. Derivative thermogravimetric (a) and differential scanning calorimetry (b) curves of cassava-starch based nanocomposites incorporated with glycerol and 0 (F0), 1 (F1), 3 (F3) or 5% (F5) of cellulose nanofibers extracted from sisal. [Color figure can be viewed at wileyonlinelibrary.com]

Thermal Properties

Thermogravimetry (TG). Overall, the nanocomposite components were decomposed between 257.46 and 352.81 °C (Table I). The addition of cellulose nanofibers reduced the initial degradation temperature and the weight loss after the thermal event [Figure 5(a)]. This suggests that the thermal stability of the nanocomposites decreased as a result of increased cellulose nanofiber concentrations. The same behavior was observed by Kaushik *et al.*,[42] who reported decreased onset degradation temperature when cellulose nanofiber content increased from 10 to 15%. According to the authors, this could be attributed to the decreased flexibility of amylopectin chains when crystalline cellulose was present.

It was also observed that the temperature of maximum degradation rate decreased as cellulose nanofiber content was increased. Although this trend was not true for the film containing 5% of cellulose nanofibers, the maximum degradation temperature was even lower than in the control formulation (F0), corroborating that the thermal stability of the films decreased upon cellulose nanofiber addition.

Differential Scanning Calorimetry (DSC). All DSC curves [Figure 5(b)] presented a typical endothermic peak that is attributable to starch gelatinization. According to Table II, the onset temperatures (T_{onset}) of all formulations were fairly close (between 29 and 32 °C). However, the nanofiber-added formulations had a melting temperature peak ($T_{melting}$) greater than the control. This suggests that the addition of nanoparticles might increase the melting temperature of the nanocomposites. Similar behavior was observed by Savadekar and Mhaske,[43] who reported that the addition of 1% of nanocellulose extracted from cotton fibers into glycerol-plasticized starch composites slightly shifted DSC curve to the right (i.e., towards higher temperatures). This means that melting temperature was higher when compared to the control.

CONCLUSIONS

The results presented here show that the incorporation of cellulose nanofibers extracted from sisal into glycerol-plasticized

cassava starch-based films is feasible to produce nanocomposites featuring improved mechanical, barrier, and thermal properties. Both Young's modulus and maximum tensile force were increased by the cellulose nanofiber addition and increasing nanofiber concentrations. Contrastingly, their elongation at break, swelling degree in water, and water vapor permeability were lessened. These results are compatible with the fundamental aspects of packaging materials intended for food shelf life extension. The combination of cassava starch (as the polymer matrix), glycerol (as the plasticizer), and cellulose nanofibers (as fillers for reinforcement purposes) was shown to possibly lead to nanocomposite films with superior barrier and mechanical properties. As a result, this study can help pave the way for the large scale production of novel environmentally friendly packaging materials.

ACKNOWLEDGMENTS

The authors thank the financial support provided by the National Council for Scientific and Technological Development (CNPq). J. S. Santana, C. C. Pola, and C. G. Otoni received scholarships from Bahia (FAPESB), Minas Gerais (FAPEMIG), and São Paulo (FAPESP, grant #2014/23098-9) Research Foundations, respectively. J. S. Santana, J. M. Rosário, and C. C. Pola have designed the experiments as well as acquired and analyzed the data. J. S. Santana, C. G. Otoni, and R. S. Cruz have designed the experiments, interpreted the data, and drafted the article. N. F. F. Soares, G. P. Camilloto, and R. S. Cruz have designed the research and revised the paper critically. All authors have approved the submitted version of the article.

REFERENCES

1. Scarfato, P. D.; Maio, L.; Incarnato, L. *J. Appl. Polym. Sci.* **2015**, *132*, DOI: 10.1002/app.42597.
2. Glenn, G. M.; Orts, W. J.; Nobes, G. A. R. *Ind. Crops Prod.* **2001**, *14*, 201.
3. Rahman, M. M.; Netravali, A. N.; Tiimob, B. J.; Apalangya, V.; Rangari, V. K. *J. Appl. Polym. Sci.* **2016**, *133*, DOI: 10.1002/app.43477.
4. Shogren, R. L.; Lawton, J. W.; Doane, W. M.; Tiefenbacher, K. F. *Polymer* **1998**, *39*, 6649.
5. Shogren, R. L.; Lawton, J. W.; Tiefenbacher, K. F. *Ind. Crops Prod.* **2002**, *16*, 69.
6. Tiefenbacher, K. F. *J. Macromol. Sci. Chem.* **1993**, *30*, 727.
7. de Moraes, J. O.; Scheibe, A. S.; Sereno, A.; Laurindo, J. B. *J. Food Eng.* **2013**, *119*, 800.
8. Detduangchan, N.; Sridach, W.; Wittaya, T. *Int. Food Res. J.* **2014**, *21*, 1225.
9. Liu, D. G.; Zhong, T. H.; Chang, P. R.; Li, K. F.; Wu, Q. L. *Bioresour. Technol.* **2010**, *101*, 2529.
10. Ma, X.; Yu, J. *Starch/Staerke* **2004**, *56*, 545.
11. Shimazu, A. A.; Mali, S.; Grossmann, M. V. E. *Semina: Cienc. Agrar.* **2007**, *28*, 79.
12. Kumar, A. P.; Singh, R. P. *Bioresour. Technol.* **2008**, *99*, 8803.
13. Jorfi, M.; Foster, E. J. *J. Appl. Polym. Sci.* **2015**, *132*, DOI: 10.1002/app.41719.
14. Berthet, M. A.; Angellier-Coussy, H.; Guillard, V.; Gontard, N. *J. Appl. Polym. Sci.* **2016**, *133*, DOI: 10.1002/app.42528.
15. Lima, M. M. D.; Borsali, R. *Macromol. Rapid Commun.* **2004**, *25*, 771.
16. Samir, M. A. S. A.; Alloin, F.; Dufresne, A. *Biomacromolecules* **2005**, *6*, 612.
17. Rosa, M. F.; Medeiros, E. S.; Malmonge, J. A.; Gregorski, K. S.; Wood, D. F.; Mattoso, L. H. C.; Glenn, G.; Orts, W. J.; Imam, S. H. *Carbohydr. Polym.* **2010**, *81*, 83.
18. Pasquini, D.; Teixeira, E. D.; Curvelo, A. A. D.; Belgacem, M. N.; Dufresne, A. *Ind. Crops Prod.* **2010**, *32*, 486.
19. da Silva, J. B. A.; Pereira, F. V.; Druzian, J. I. *J. Food Sci.* **2012**, *77*, N14.
20. de Moura, M. R.; Avena-Bustillos, R. A.; McHugh, T. H.; Wood, D. F.; Otoni, C. G.; Mattoso, L. H. C. *J. Food Eng.* **2011**, *104*, 154.
21. Cao, X. W.; Ding, B.; Yu, J. Y.; Al-Deyab, S. S. *Carbohydr. Polym.* **2012**, *90*, 1075.
22. Alves, J. S.; dos Reis, K. C.; Menezes, E. G. T.; Pereira, F. V.; Pereira, J. *Carbohydr. Polym.* **2015**, *115*, 215.
23. Reddy, J. P.; Rhim, J. *Carbohydr. Polym.* **2014**, *110*, 480.
24. Lee, S.; Mohan, D. J.; Kang, I.; Doh, G.; Lee, S.; Han, S. O. *Fibers Polym.* **2009**, *10*, 77.
25. Fang, Y.; Tung, M. A.; Britt, I. J.; Yada, S.; Dalgleish, D. G. *J. Food Sci.* **2002**, *67*, 188.
26. Shiku, Y.; Hamaguchi, P. Y.; Tanaka, M. *Fish. Sci. (Tokyo, Jpn.)* **2003**, *69*, 1026.
27. Han, J. H.; Floros, J. D. *J. Plast. Film Sheeting* **1997**, *13*, 287.
28. Woggum, T.; Sirivongpaisal, P.; Wittaya, T. *Int. J. Biol. Macromol.* **2014**, *67*, 490.
29. Jipa, I. M.; Stoica-Guzun, A.; Stroescu, M. *LWT Food Sci. Technol.* **2012**, *47*, 400.
30. American Society for Testing and Materials (ASTM). ASTM Standard E96/E96M-12, Standard Test Method for Water Vapor Transmission Rate of Materials; ASTM International: Philadelphia, **2012**.
31. American Society for Testing and Materials (ASTM). ASTM Standard D638-09, Standard Test Method for Tensile Properties of Plastics; ASTM International: Philadelphia, **2009**.
32. American Society for Testing and Materials (ASTM). ASTM Standard E1306-90(2008)e1, Standard Test Method for Slow Rate Penetration Resistance of Flexible Barrier Films and Laminates; ASTM International: Philadelphia, **2008**.
33. Chang, P. R.; Jian, R. J.; Zheng, P. W.; Yu, J. G.; Ma, X. F. *Carbohydr. Polym.* **2010**, *79*, 301.
34. Elazzouzi-Hafraoui, S.; Nishiyama, Y.; Putaux, J. L.; Heux, L.; Dubreuil, F.; Rochas, C. *Biomacromolecules* **2008**, *9*, 57.
35. Zhou, Y. M.; Fu, S. Y.; Zheng, L. M.; Zhan, H. Y. *eXPRESS Polym. Lett.* **2012**, *6*, 794.
36. Espitia, P. J. P.; Soares, N. D. F.; Teofilo, R. F.; Coimbra, J. S. D.; Vitor, D. M.; Batista, R. A.; Ferreira, S. O.; de

Andrade, N. J.; Medeiros, E. A. A. *Carbohydr. Polym.* **2013**, *94*, 199.

37. Khan, A.; Khan, R. A.; Salmieri, S.; Le Tien, C.; Riedl, B.; Bouchard, J.; Chauve, G.; Tan, V.; Kamal, M. R.; Lacroix, M. *Carbohydr. Polym.* **2012**, *90*, 1601.
38. Garcia, N. L.; Ribba, L.; Dufresne, A.; Aranguren, M. I.; Goyanes, S. *Macromol. Mater. Eng.* **2009**, *294*, 169.
39. Yu, L.; Dean, K.; Li, L. *Prog. Polym. Sci.* **2006**, *31*, 576.
40. Kalia, S.; Dufresne, A.; Cherian, B. M.; Kaith, B. S.; Averous, L.; Njuguna, J.; Nassiopoulos, E. *Int. J. Polym. Sci.* **2011**, *2011*, 837875.
41. Anglès, M. N.; Dufresne, A. *Macromolecules (Washington, DC)* **2001**, *34*, 2921.
42. Kaushik, A.; Singh, M.; Verma, G. *Carbohydr. Polym.* **2010**, *82*, 337.
43. Savadekar, N. R.; Mhaske, S. T. *Carbohydr. Polym.* **2012**, *89*, 146.